Sequential melting of deep crustal sources in a rift system: An example from the Southern Tibet

Li E Gao[1], Lingsen Zeng[1], Linghao Zhao[2], and Li-Long Yan[3]

[1]Institute of Geology, Chinese Academy of Geological Sciences
[2]National Research Center for Geoanalysis, Chinese Academy of Geological Sciences
[3]Chinese Academy of Geological Sciences

November 26, 2022

Abstract

How the continental crust responds geochemically to progressive extension is one of the interesting questions. The Southern Tibet Rift System (STRS) is one of the active extensional structures. The Yardoi gneiss dome, located within STRS, consists of at least four suites of Miocene granites. As crystallization ages become younger, they are characterized by decrease in ?Nd(t) and Sr/Y, but increase in 87Sr/86Sr(t) and Rb/Sr. Such temporal trends could be explained by sequential partial melting of first the mafic lower crustal rocks and then progressively shallower metasedimentary rocks. Together with literature data, from north to south along STRS, as the extension proceeds and the heat moves upward, sequential partial melting is common to produce Miocene magmatic rocks. The processes documented in the southern Tibet might be common in other extensional provinces and provides a new insight to unravel the mechanisms for the generation of geochemical variations in contemporaneous granites.

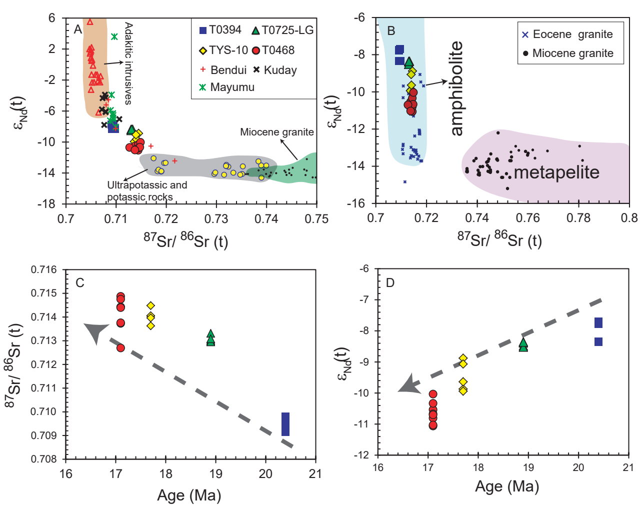

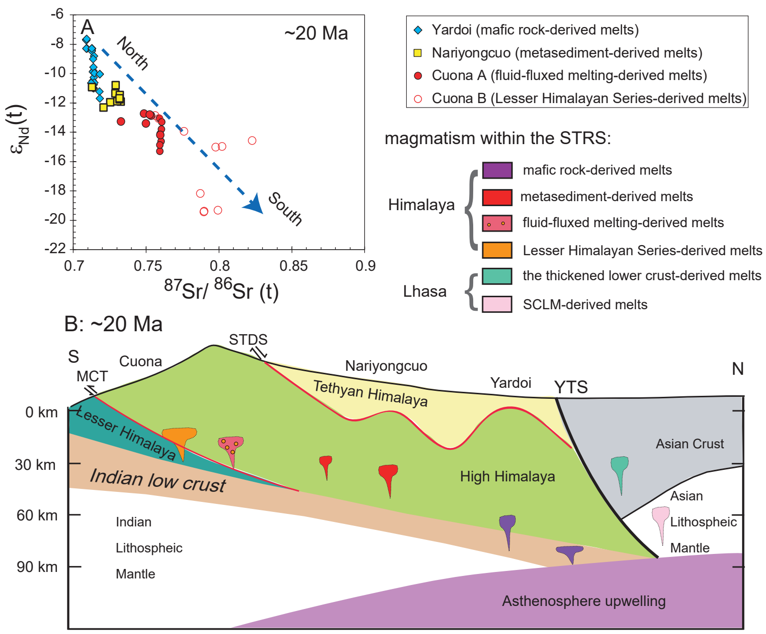
A
~20 Ma
North
South
$\varepsilon_{Nd}(t)$
$^{87}Sr/^{86}Sr$ (t)
Yardoi (mafic rock-derived melts)
Nariyongcuo (metasediment-derived melts)
Cuona A (fluid-fluxed melting-derived melts)
Cuona B (Lesser Himalayan Series-derived melts)
magmatism within the STRS:
Himalaya
mafic rock-derived melts
metasediment-derived melts
fluid-fluxed melting-derived melts
Lesser Himalayan Series-derived melts
Lhasa
the thickened lower crust-derived melts
SCLM-derived melts
B: ~20 Ma
S
N
MCT
Cuona
STDS
Nariyongcuo
Yardoi
YTS
Tethyan Himalaya
Lesser Himalaya
Indian low crust
High Himalaya
Asian Crust
Asian Lithospheic Mantle
Indian Lithospheic Mantle
Asthenosphere upwelling
0 km
30 km
60 km
90 km

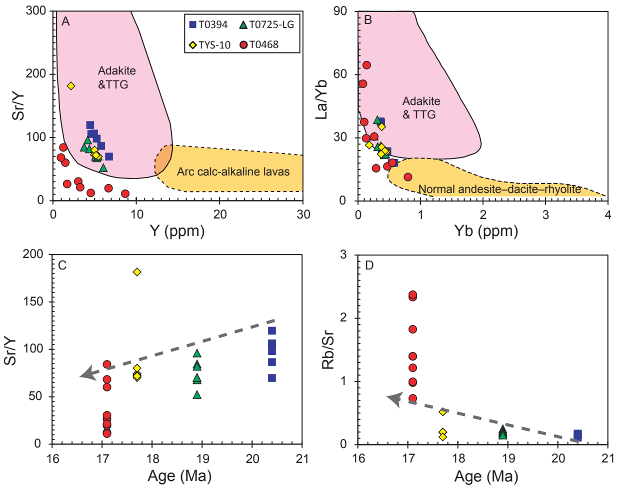
A
T0394
T0725-LG
TYS-10
T0468
Adakite
&TTG
Arc calc-alkaline lavas
Sr/Y
Y (ppm)
B
Adakite
& TTG
Normal andesite–dacite–rhyolite
La/Yb
Yb (ppm)
C
Sr/Y
Age (Ma)
D
Rb/Sr
Age (Ma)

Sequential melting of deep crustal sources in a rift system: An example from the Southern Tibet

Li-E Gao[1]*, Lingsen Zeng[1], Linghao Zhao[2], Lilong Yan[1]

[1]Institute of Geology, Chinese Academy of Geological Sciences, Beijing 100037, China.

[2] National Research Center for Geoanalysis, Chinese Academy of Geological Sciences, Beijing 100037, China.

ABSTRACT

How the continental crust responds geochemically to progressive extension is one of the interesting questions. The Southern Tibet Rift System (STRS) is one of the active extensional structures. The Yardoi gneiss dome, located within STRS, consists of at least four suites of Miocene granites. As crystallization ages become younger, they are characterized by decrease in $\varepsilon_{Nd}(t)$ and Sr/Y, but increase in $^{87}Sr/^{86}Sr(t)$ and Rb/Sr. Such temporal trends could be explained by sequential partial melting of first the mafic lower crustal rocks and then progressively shallower metasedimentary rocks. Together with literature data, from north to south along STRS, as the extension proceeds and the heat moves upward, sequential partial melting is common to produce Miocene magmatic rocks. The processes documented in the southern Tibet might be common in other extensional provinces and provides a new insight to unravel the mechanisms for the generation of geochemical variations in contemporaneous granites.

Keywords: sequential melting, high Sr/Y ratios, granites, extension, rift, the southern Tibet

INTRODUCTION

In various tectonic settings, impingement of a thermal pulse could be induced by breakoff of a subducting slab, extension and rifting or delamination of a dense thickened continental lithosphere (Gorti, 2009; Rychert et al., 2012). All these processes could gradually warm up the continental crust, and eventually trigger partial melting of different fertile components and produce granitic melts with vastly different mineral and chemical signatures depending on the pressure and temperature conditions achieved. In the upwelling regions associated with continental rifting, the depth of melting decreases with time (Wendlandt and Morgan, 1982), which conceptually could be proceeded by sequential melting. Sequential melting of a vertical column of continental crust triggered by the ascent of a thermal pulse has been suggested to generate co-existing granitic rocks with distinct mineral assemblage and isotope compositions (Holtz and Barbey, 1991; Nabelek et al., 1992; Greenfield et al., 1998; Gutiérrez-Alonso et al., 2011; Carvalho et al., 2012). However, how the geochemical nature of granitic melts changes through such a process is still poorly documented. The Southern Tibet Rift System (STRS), one of the active extensional structures in the southern Tibet, is composed of a series of nearly north-south trending rift valleys from the Lhasa terrain down to the Himalayan belt, and represents ongoing

E-W orogen-parallel extension (Taylor and Yin, 2009; Nagy et al., 2015). Instability analysis suggests that the mantle lithosphere must have been involved in E-W extension (Yin, 2000). In the Lhasa terrain, extension has induced partial melting of the enriched subcontinental lithosphere (SCLM) as well as the thickened lower crust (Chung et al., 2003; Hou et al., 2004; Liu et al., 2014; Guo et al., 2019). In the Himalayan belt, East-West extension could be dated back to ~19 Ma (Mitsuishi et al., 2012; Zhang et al., 2012; Nagy et al., 2015) and resulted in the exhumation of a number of gneiss domes in the Tethyan Himalaya (Xu et al., 2013; Wang et al., 2018). If such process is common to all the branches of STRS from north to south, then it is conceivable that the basement rocks in the Himalayan belt should experience progressive heating as the extension proceeds. Whether such a heating could induce partial melting of lower crustal rocks is one of the interesting questions deserved careful investigations. How the intermediate to lower crustal rocks response physically as well as geochemically to such extension is one of the poorly constrained problems. The Yardoi gneiss dome, located within the Sangri-Cuona rift, one of the branches of STRS (Fig. 1A, Taylor et al., 2009), could have experienced progressive heating due to extension and exhumation and provides us an excellent opportunity to address the questions posed above.

In this contribution, we present geochemical as well as geochronological data of four suites of Miocene granites from the Yardoi gneiss dome. These data together with literature data from the Nariyongcuo and the Cuona within the Sangri-Cuona rift, and from those rift valleys in the Lhasa terrane, are used to pain a detailed picture of the variations in the melting reactions of deep crustal rocks within STRS.

GEOLOGICAL SETTING

The Yardoi gneiss dome (YGD) is located within the Sangri-Cuona rift and in the easternmost of the Tethyan Himalaya (Fig. 1A). From the core to the margin, it consists of Eocene granites (Zeng et al. 2015) in the core, high-grade metamorphic rocks, mediate-grade garnet graphite schist and intruding Oligocene and Miocene granitic dykes (Zeng et al. 2011) toward the margin, followed by the overlying Tethyan sedimentary rocks (Fig. 1B). In addition, minor sheared two-mica granitic rocks of ages ~43-44 Ma occur in the Dala and Quedang area and subvolcanic porphyritic leucogranite dikes or plugs of ages 41.4 Ma (Zeng et al., 2015) occur along the E-W trending valley from Qiaga to Longzi (Fig. 1B). The Eocene granitic rocks were derived from partial melting of amphibolite under thickened crustal conditions (Zeng et al., 2011; Hou et al., 2012). In the mantle, some meter-wide leucogranitic dykes recorded U–Pb ages of 20~17 Ma (Gao et al., 2020), whereas, the geochemical nature and the formation mechanism have not been described before. We sampled four suites of granite T0394, T0725-LG, TYS-10, and T0468 as shown in Fig. 1B. They consist of quartz, plagioclase, muscovite, K-feldspar and accessory phases of zircon, apatite, and monazite (Fig. S1). Except T0468, other granites contain 5% biotite.

RESULTS

All the zircons from the four suites of granites show oscillatory zoning. Weighted mean ages are 20.4 ± 0.4 Ma, 18.9 ± 0.2 Ma, 17.7± 0.1 Ma, 17.1 ± 0.1 Ma for T0394, T0725-LG, TYS-10, and T0468, respectively (Fig. S2, data for T0394 are from Zeng et al., 2019). Though the zircons have low Th/U ratios (<0.25, Table S1), the well-developed oscillatory zoning indicates that they were crystallized from granitic melt, therefore, we interpret these ages as the timing of crystallization for these granites.

The four suites of granites have similar geochemical natures in major elements (Fig. S3, data for the granite T0394 are from Zeng et al., 2019) and are characterized by (1) high SiO_2 (71.6–76.2 wt%), Al_2O_3 (13.7–16.3 wt%) and Na_2O (4.2–5.9 wt%); (2) low K_2O (1.1–3.7 wt%), CaO (0.7–1.8 wt%), FeO (<1.4 wt%), MgO, P_2O_5; and (3) relatively high Na_2O/K_2O (1.19–5.10) and high A/CNK (1.06–1.31) ratios, which indicate that they are Na-rich and peraluminous granite. As compared to the other samples, T0468 have relatively higher SiO_2, but lower CaO, FeO* and P_2O_5 (Fig. S3).

In primitive mantle–normalized spider diagrams (Fig. S4), T0394, T0725-LG and TYS-10 share similar geochemical characteristics, with striking negative anomalies in Nb, Ta, P, Ti, and Y along with slightly positive anomalies in Sr. In contrast, T0468 samples are characterized by striking negative anomalies in P and Ti alongside slightly negative anomalies in Nb, Sr, Zr and Y. Except sample T0468, the others have relatively high Sr (316–536 ppm) and La (8.0–13.8 ppm), but low Y (2.2–6.7 ppm) and Yb (<0.6 ppm), and thus relatively high Sr/Y ratios (52.2–181.6) and La/Yb ratios (18.0–38.5). In the Sr/Y–Y and La/Yb–Yb diagram, all three suites of granite are plotted within the adakite field (Fig. 2). In particular, most samples in T0468 have lower Sr/Y ratios (<30.4) at similar Y concentrations (Fig. 2A), and lower

La/Yb ratios (<18.2) at similar Yb concentrations (Fig. 2B), respectively. In additional, trace element ratios of Rb/Sr, Nb/Ta and Zr/Hf are apparently different. T0468 have high Rb/Sr (0.7–2.4) and low Zr/Hf (15.8–26.2), Nb/Ta (4.5–8.7). Compared to T0468, others are characterized by lower Rb/Sr ratios (<0.3), but higher Zr/Hf (22.3–32.7) and Nb/Ta (6.9–15.5). Interestingly, as crystallization ages become younger, Sr/Y ratios decrease, but Rb/Sr ratios increase (Fig. 2C, D).

All the granites are enriched in light REEs (LREE) and depleted in heavy REEs (HREE), however, T0468 have relatively lower contents of LREE than others, and more weakly degree of fractionation LREE over HREE (Fig. S4). The Eu anomalies display significant difference. T0468 are characterized by pronounced negative Eu anomalies (Eu/Eu*<0.56) and negative Nd anomalies (Nd/Nd*=0.81–0.90), whereas, others have relatively higher and variable Eu anomalies (Eu/Eu* = 0.90–1.25) and limited negative Nd anomalies (Nd/Nd*=0.85–0.96) (Table S2).

The granites display a large variation in Sr and Nd isotope ratios, but all feature relatively radiogenic $^{87}Sr/^{86}Sr(t)$ (0.7091–0.7149) and unradiogenic $\varepsilon_{Nd}(t)$ (–11.1 to –7.7; Fig. 3). There is regularity in variations of Sr and Nd isotope ratios for YGD Miocene granites. As crystallization ages become younger, $\varepsilon_{Nd}(t)$ value decrease, but $^{87}Sr/^{86}Sr(t)$ increase (Fig. 3C, 3D).

DISCUSSION

The data presented above demonstrate that except sample T0468, the other three Miocene granites in the YGD are Na-rich and peraluminous granite with high Sr/Y and La/Yb ratios. Compared with the others, T0468 have different geochemical natures and are characterized by (1) higher SiO_2, lower CaO, FeO*, TiO_2 and P_2O_5; (2) higher Rb and Ta, lower Sr, LREE, Zr, and Ti, thus higher Rb/Sr but lower Sr/Y, La/Yb, Zr/Hf and Nb/Ta ratios; (3) pronounced negative Eu anomalies and negative Nd anomalies. These differences (Fig. S4) and systematic relationships in major and trace elements (Fig. S5) suggest that T0468 had suffered from various degrees of fractional crystallization of plagioclase, zircon, monazite, apatite, and Ti-rich mineral phases, which is common to the Himalaya high silica leucogranites (Liu et al., 2019), whereas, others seem to be more primitive and represent the more faithful melt compositions. In addition, T0468 shows a large variation in Rb/Sr ratios, but no linear relationship between Rb/Sr and $^{86}Sr/^{87}Sr$ ratios (Fig. S5), which indicates that fractional crystallization has negligible effects on their Sr-Nd isotope compositions.

E-W extension in the southern Tibet results in the formation of adakitic and potassic-ultrapotassic magmatic rocks (Chung et al., 2003). The adakitic magmas were formed by a complex mechanism involving partial melting of mafic materials in a thickened lower crust with input of enriched mantle and upper crust components (Hou et al., 2004). Potassic-ultrapotassic rocks were derived from a metasomatized subcontinental lithospheric mantle (SCLM) with additional contributions from thickened juvenile lower crust or ancient basement (Liu et al., 2014). This lower-crustal melting required a significantly elevated geotherm, which is attributed to removal of the tectonically thickened lithospheric mantle at depth (Chung et al., 2003), followed by E–W extension setting associated with Miocene plateau uplift (Liu et al., 2014). The YGD is located within the Sangri-Cuona rift (Fig. 1A, Taylor et al.,

2009) and the basement rocks should have experienced progressive heating as the extension proceeds. As compare to above rocks in the Lhasa block, the four suites of Yardoi Miocene granites are characterized by intermediate $\varepsilon_{Nd}(t)$ and $^{87}Sr/^{86}Sr(t)$ (Fig. 3A). As compare to the nearly contemporaneous granites in the Himalayan orogenic belt, the Yardoi Miocene granites have different Sr–Nd isotope compositions, in contrast with similar Sr but elevated Nd isotope compositions to those in the Eocene granites (Fig. 3B). Therefore, the Miocene granites in the YGD could be derived from partial melting of lower crustal material during E-W extension. Occurrence of primary high Sr/Y granites in an orogenic belt requires a mafic source component in deeper crustal levels. Mafic materials that are responsible for these granites include (1) subcontinental mantle; (2) lower crustal mafic materials (amphibolite or recently underplated basaltic material); or (3) subducting Indian continental slab. The geochemical natures of low MgO (<0.65 wt %), Cr (<21 ppm), Ni (<12 ppm) in these Yardoi Miocene granites rule out mantle materials as their sources. The relatively elevated Sr isotope compositions with $^{87}Sr/^{86}Sr$ ratios of 0.7091~0.7149 and negative $\varepsilon_{Nd}(t)$ of -11.1~-7.7 could be explained by they represent melts derived from mafic components in the subducting Indian continental slab (Fig. 3). The close match in Sr and Nd isotope compositions between the Yardoi Miocene granites and the amphibolites are consistent with their derivation primarily from amphibolite (Fig. 3B). In addition, as crystallization ages become younger, from 20.4 Ma to 17.1 Ma, $\varepsilon_{Nd}(t)$ value decrease but $^{87}Sr/^{86}Sr(t)$ increase (Fig. 3C, 3D). The systemic variations in the age of formation and the Sr–Nd isotope compositions suggest that there are at least two types of source rocks. These granites should be produced by mixing of amphibolite-derived melts with metasediment-derived melts. As the extension proceeds, source regimes change from more deeply seated amphibolite toward to shallower metasedimentary rocks. This also could explain the variations in their Sr/Y and Rb/Sr ratios (Fig. 2C, 2D).

Recently, other Miocene high Sr/Y granites were reported in other gneiss domes within the Himalayan belt (Ji et al., 2019; Lin et al., 2020). They have similar Sr–Nd isotope compositions to the Miocene granites in the YGD (Fig. 3A). Occurrences of Miocene high Sr/Y granites imply that the Himalayan belt could have experienced a major episode of melting of lower crustal rock. Additionally, the Miocene granite in the YGD are high-temperature ones (~850 °C, Gao et al., 2020). Meanwhile, Miocene ultrahigh temperature metamorphism is reported in the Himalaya belt (900–970 °C, Wang et al., 2021). These high-temperature geological events require an extra heat source which would probably be provided by upwelling of asthenospheric mantle accompanied the E-W extension (Gao et al., 2020; Wang et al., 2021; Shi et al., 2020). Therefore, partial melting of the lower crust was most likely triggered by Miocene E-W extension in southern Tibet with heat source from the upwelling of asthenospheric mantle.

Sequential partial melting is a model proposed by Holtz and Barbey (1991) who explained the genesis of granitic partial melts segregated from the same melting zone during progressive heating. Early crustal thickening followed by later extension and mantle upwelling could induce similarly progressive heating and trigger progressive partial melting, which are characterized by early melting at elevated pressure conditions overtaken by progressive much shallower melting (Gutiérrez-Alonso et al., 2011; Carvalho et al., 2012). From north to south along Sangri-Cuona rift, different granites with various geochemical natures were derived from mafic rock, fluid-absent melting and fluid-fluxed melting of metasediment (Fig 4A, Gao et al., 2017). Therefore, similar to those processes after the slab breakoff (Atherton and Ghani, 2002; Magni et al., 2017), as the extension proceeds and the heat conduction moves upward into the shallower level, sequential partial melting of first subcontinental lithospheric mantle, then the mafic lower crustal rocks and finally progressively shallower metasedimentary rocks could produce similar variations in the chemical as well as isotopic compositions in the Miocene magmatic rocks within the STRS (Fig. 4B). The above processes might be common in other extensional provinces (e.g., East Africa rift, Basin and Range Province) and provides a new insight to unravel the mechanisms for the generation of the geochemical and isotopic variations in nearly contemporaneous granitic rocks.

ACKNOWLEDGMENTS

This work was supported by the Second Tibetan Plateau Scientific Expedition and Research (grant 2019QZKK0702), the National Science Foundation of China (grant 41873023&92055202), National key Research and Development plan (grant number 2021YFC2901901), and China Geological Survey (grant DD20221817&DD20221630).

Data Availability Statement

Data are published separately and are available under the https://doi.org/10.5281/zenodo.6862153

Figure 1. A: Simplified geologic map of the Himalayan orogenic belt, southern Tibet. B: Simplified geological map of the Yardoi area. STRS: Southern Tibet Rift System; NHGD: Northern Himalayan Gneiss Dome.

Figure 2. Trace elements characteristics of the Yardoi Miocene leucogranites.

Figure 3. A: Sr–Nd isotope systematics of the magmatic rocks lied in NSTR, containing Miocene high Sr/Y granite from the Yardoi, Mayum (Lin et al., 2020), Kuday (King et al., 2007) and Bendui (Ji et al., 2019) in the Himalayan belt, adakitic intrusives (Hou et al., 2004) and the ultrapotassic and potassic rocks (Liu et al., 2014) in the Lhasa terrain. B: Sr–Nd isotope systematics of the Eocene granites and other Miocene granites, as well as amphibolite and metapelite in the Himalayan orogenic belt (Zeng et al., 2015). C-D: The relationship between crystallization ages and Sr-Nd isotope compositions of the Yardoi Miocene granite.

Figure 4. A: Sr–Nd isotope systematics of the ~20 Ma granites from north to south within Sangri-Cuona rift (date from Gao et al., 2019 and our unpublished data). B: the model for the magmatism induced by E-W extension within the NSTR. YTS: Yalung-Tsangpo suture; STDS: Southern Tibet Detachment System; MCT: Main Central Thrust.

Supplemental Material. Figures S1- S5, and Table S1- S2.

REFERENCES CITED

Atherton, M.P., and Ghani, A.A., 2002, Slab breakoff: a model for Caledonian, Late Granite syn-collisional magmatism in the orthotectonic (metamorphic) zone of Scotland and Donegal, Ireland. Lithos, v. 62, p. 65–85.

Carvalho, P.C.S., Neiva, A.M.R., Silva, M.M.V.G., and Corfu, F., 2012, A unique sequential melting mechanism for the generation of anatectic granitic rocks from the Penafiel area, northern Portugal. Lithos, v. 155, p. 110–124.

Chung, S.L., Liu, D.Y., Ji, J.Q., Chu, M.F., Lee, H.Y., Wen, D.J., Lo, C.H., Lee, T.Y., Qian, Q., and Zhang, Q., 2003, Adakites from continental collision zones: melting of thickened lower crust beneath southern Tibet. Geology, v. 31, p. 1021–1024.

Gao, P., Zheng, Y.F., Mayne, M.J., and Zhao, Z.F., 2020, Miocene high-temperature leucogranite magmatism in the Himalayan orogen. GSA Bulletin. v. 133(3–4), p. 679–690, doi: 10.1130/b35691.1.

Gao, L.E., Zeng, L.S., Gao, J.H., Zhao, L.H., Hou, K.J., and Tang S.H., 2017, The Miocene leucogranite in the Nariyongcuo Gneiss Dome, southern Tibet: Products from melting metapelite and fractional crystallization. Acta Petrologica Sinica, v. 33(8), p. 2395–2411.

Gorti, G., 2009, Continental rift evolution: from rift initiation to incipient break-up in the main Ethiopian rift, East Africa. Earth Science Reviwes, v. 96, p. 1–53.

Greenfield, J.E., Clarke, G.L., and White, R.W., 1998, A sequence of partial melting reactions at Mt Stafford, central Australia. Journal of Metamorphic Geology, v.

16, p. 363–378.

Guo, Z.F., and Wilson, M., 2019, Late Oligocene–early Miocene transformation of postcollisional magmatism in Tibet. Geology, v. 47, p. 1–5, doi: 10.1130 /G46147.1.

Gutiérrez-Alonso, G., Fernández-Suárez, J., Jeffries, T.E., Johnston, S.T., Pastor-Galán, D., Murphy, J.B., Franco, M.P., and Gonzalo, J.C., 2011, Diachronous post-orogenic magmatismwithin a developing orocline in Iberia, European Variscides. Tectonics, v. 30, p. TC5008.

Holtz, F., and Barbey, P., 1991, Genesis of peraluminous granites. II. Mineralogy and chemistry of the Tourem complex (northern Portugal). Sequential melting vs. restite unmixing. Journal of Petrology, v. 32, p. 959–978.

Hou, Z.Q., Gao, Y. F., Qu, X.M., Rui, Z. Y., and Mo, X.X., 2004, Origin of adakitic intrusives generated during mid-Miocene east–west extension in southern Tibet. Earth Planetary Science Letters, v. 220 (1–2), p. 139–155.

Hou, Z.Q., Zheng, Y.C., Zeng, L.S., Gao, L.E., Huang, K.X., Li, W., Li, Q.Y., Fu, Q., Liang, W., and Sun, Q.Z., 2012, Eocene–Oligocene granitoids in southern Tibet: constraints on crustal anatexis and tectonic evolution of the Himalayan orogen. Earth Planetary Science Letters, v. 349–350, p. 38–52.

Ji, W.Q., Wu, F.Y., Liu, X.C., Liu, Z.C., Zhang, C., Liu, T., Wang, J.G., and Paterson, S.R., 2020, Pervasive Miocene melting of thickened crust from the Lhasa terrane to Himalaya, southern Tibet and its constraint on generation of Himalayan leucogranites: Geochimica et Cosmochimica Acta, v. 278, p. 137–156, doi:10.1016/j.gca.2019.07.048.

King J., Harris N., Argles T., Parrish R., Charlier B., Sherlock S., and Zhang H.F., 2007, First field evidence of southward ductile flow of Asian crust beneath southern Tibet. Geology, v. 35, p. 727–730.

Lin, C., Zhang, J.J., Wang, X.X., Huang, T.L., Zhang, B., and Fan, Y.S., 2020, Himalayan Miocene adakitic rocks, a case study of the Mayum pluton: Insights into geodynamic processes within the subducted Indian continental lithosphere and Himalayan mid-Miocene tectonic regime transition. GSA Bulletin, doi: 10.1130/b35640.1.

Liu, D., Zhao, Z.D., Zhu, D.C., Niu, Y.L., DePaolo, D.J., Harrison, T.M., Mo, X.X., Dong, G.C., Zhou, S., Sun, C.G., Zhang, Z.C., and Liu, J.L., 2014, Postcollisional potassic and ultrapotassic rocks in southern Tibet: Mantle and crustal origins in response to India-Asia collision and convergence. Geochimica et Cosmochimica Acta, v. 143, p. 207–231.

Liu, Z.C., Wu, F.Y., Liu, X.C., Wang, J.G., Yin, R., Qiu, Z.L., Ji, W.Q., and Yang, L., 2019, Mineralogical evidence for fractionation processes in the Himalayan leucogranites of the Ramba Dome, southern Tibet. Lithos, v. 340–34, p. 71–86.

Magni, V., Allen, M.B., van Hunen, J., and Bouilhol, P., 2017, Continental underplating after slab break-off. Earth and Planetary Science Letters, v. 474, p. 59–67.

Mitsuishi, M., Simon, R.W., Aoya, M., Lee, J., and Wang, Y., 2012, E–W extension at 19 Ma in the Kung Co area, S. Tibet: Evidence for contemporaneous E–W and

N–S extension in the Himalayan orogen. Earth and Planetary Science Letters, v. 325–326, p.10–20.

Nabelek, P., Russ-Nabelek, C., and Denison, J. R., 1992. The generation and crystallization conditions of the Proterozoic Harney Peak leucogranite, Black Hills, South Dakota, USA: petrologic and geochemical constraints. Contributions to Mineralogy and Petrology, v. 110, p. 173–191.

Nagy, C., Godin, L., Antolín, B., Cottle, J., and Archibald, D., 2015, Mid-Miocene initiation of orogen-parallel extension, NW Nepal Himalaya. Lithosphere, v. 7, p. 483–502, doi:10.1130/L425.1.

Rychert, C.A., Hammond, J., Harmon, N., Kendall, J.M., Keir, D., Ebinger, C., Bastow, I.D., Ayele, A., Belachew, M., and Stuart, G., 2012, Volcanism in the Afar Rift sustained by decompression melting with minimal plume influence. Nuture Geoscience, v. 5, p. 406–409, doi: 10.1038/NGEO1455

Shi, D., Klemperer, S.L., Shi, J.Y., Wu, Z.H., and Zhao, W.J., 2020, Localized foundering of Indian lower crust in the India Tibet collision zone. Proceedings of the National Academy of Sciences, v.117(40), p. 24742–24747, doi:10.1073/pnas.2000015117.

Taylor, M., and Yin, A., 2009, Active structures of the Himalayan-Tibetan orogen and their relationships to earthquake distribution, contemporary strain field, and Cenozoic volcanism. Geosphere, v. 5, p. 199–214, Doi:10.1130/GES00217.1.

Wang, J.M., Lanari, P., Wu, F.Y., Zhang, J.J., and Yang, L., 2021, First evidence of eclogites overprinted by ultrahigh temperature metamorphism in everest east, himalaya: implications for collisional tectonics on early earth. Earth and Planetary Science Letters, v. 558(3–4), p. 116760, doi: 10.1016/j.epsl.2021.116760.

Wang, J.M., Wu, F.Y., Robatto, D., Liu, K., Zhang, J.J., and Liu, X.C., 2018, Early Miocene rapid exhumation in southern Tibet: Insights from P-T-t-D-magmatism path of Yardoi dome. Lithos, v. 304–307, p. 38–56, doi:10.1016/j.lithos.2018.02.003.

Wendlandt, R.F., and Morgan, P., 1982, Lithospheric thinning associated with rifting in East Africa. Nature, v. 298, p. 734–736.

Xu, Z., Wang, Q., Pecher, A., Liang, F.H., Qi, X.X., Cai, Z.H., Li, H.Q., Zeng, L.S., and Cao, H., 2013, Orogen-parallel ductile extension and extrusion of the Greater Himalaya in the late Oligocene and Miocene: Tectonics, v. 32, p. 191–215, doi:10.1002/tect.20021.

Yin, A., 2000. Mode of Cenozoic east-west extension in Tibet suggesting a common origin of rifts in Asia during the Indo-Asian collision: Journal of Geophysical Research: Solid Earth, v.105(B9), p. 21745–21759, doi: 10.1029/2000JB900168.

Zeng, L.S., Gao, L.E, Tang, S.H., Hou, K.J., Guo, C.L., and Hu, G.Y., 2015, Eocene magmatism in the Tethyan Himalaya, southern Tibet. In Mukherjee. S., Carosi, R., van der Beek, P.A., Mukherjee, B.K., and Robinson, D.M., (eds) Tectonics of the Himalaya. Geological Society, London, Special Publications, v. 412 (1), p. 287–316, doi:10.1144/SP412.8.

Zeng, L.S., Gao, L.E., Xie, K.J., and Liu, J., 2011, Mid-Eocene high Sr/Y granites in the Northern Himalayan Gneiss Domes: Melting thickened lower continental crust. Earth and Planetary Science Letters, v. 303, p. 251–266, doi: 10.1016/j.epsl.2011.01.005.

Zeng, L.S., Zhao, L.H., Gao, L.E., Hou, K.J., and Wang, Q., 2019. Magmatic garnet from Mid-Miocene co-genetic high Sr/Y granite and leucogranite from the Himalayan orogenic belt, southern Tibet. Acta Petrologica Sinica, v. 35(6), p. 1599–1626.

Zhang, J.J., Santosh, M., Wang, X.X., Guo, L., Yang, X.Y., and Zhang, B., 2012, Tectonics of the northern Himalaya since the India–Asia collision. Gondwana Research, v. 21(4), p. 939–960.

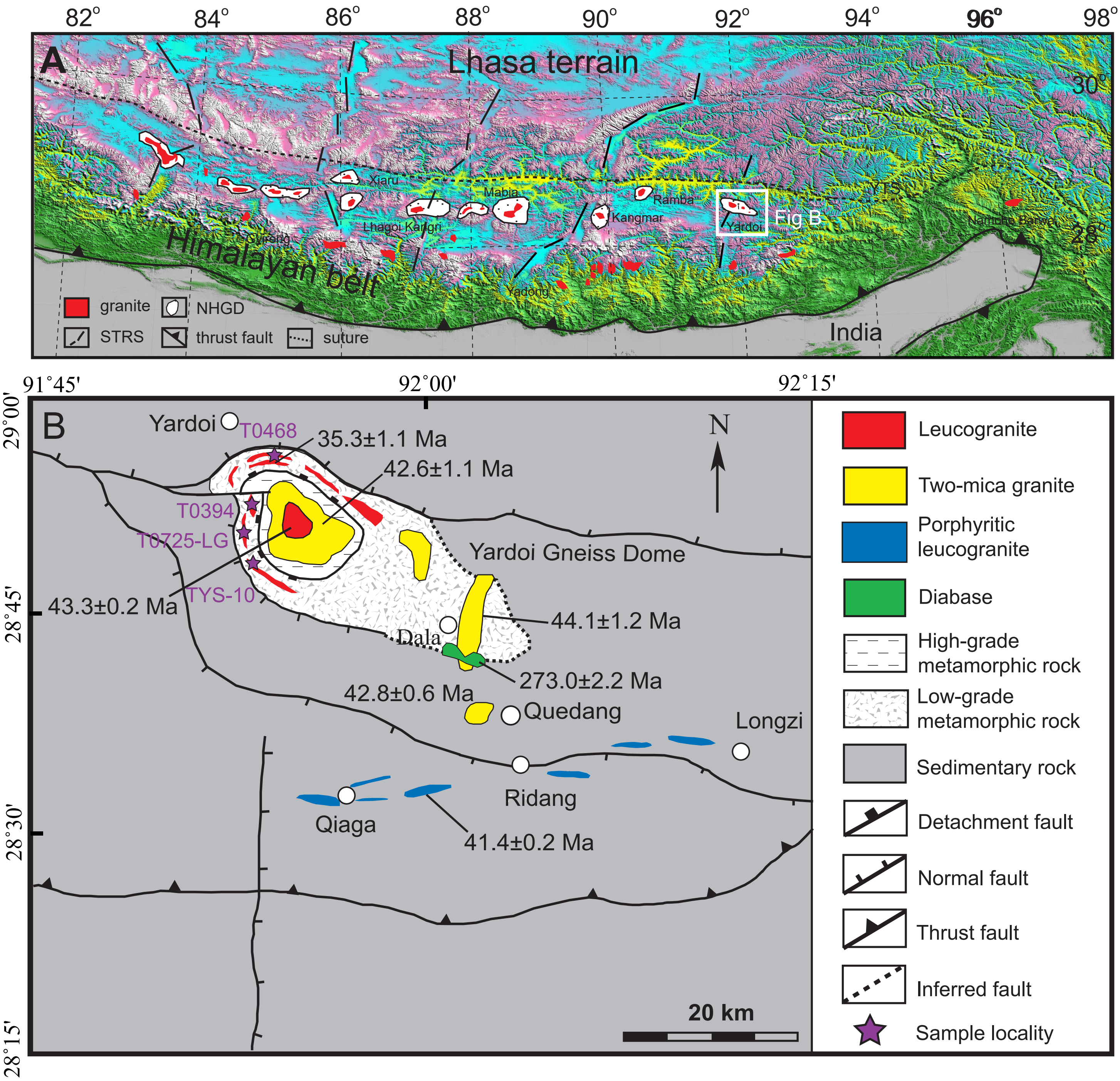

A
Lhasa terrain
Himalayan belt
India
82°
84°
86°
88°
90°
92°
94°
96°
98°
30°
28°
Xiaru
Mabja
Ramba
Kangmar
Lhagoi Kangri
Gyirong
Yadong
Yardoi
YTS
Fig B
Namche Barwa
granite
NHGD
STRS
thrust fault
suture
B
91°45'
92°00'
92°15'
29°00'
28°45'
28°30'
28°15'
Yardoi
T0468
35.3±1.1 Ma
42.6±1.1 Ma
T0394
T0725-LG
TYS-10
43.3±0.2 Ma
Yardoi Gneiss Dome
44.1±1.2 Ma
Dala
273.0±2.2 Ma
42.8±0.6 Ma
Quedang
Longzi
Ridang
Qiaga
41.4±0.2 Ma
N
20 km
Leucogranite
Two-mica granite
Porphyritic leucogranite
Diabase
High-grade metamorphic rock
Low-grade metamorphic rock
Sedimentary rock
Detachment fault
Normal fault
Thrust fault
Inferred fault
Sample locality